Inorganic Chemistry

pubs.acs.org/IC Article

Synthesis and Characterization of Tellurium Catecholates and Their *N*-Oxide Adducts

Jerod M. Kieser, Leighton O. Jones, Nathan J. Lin, Matthias Zeller, George C. Schatz, and Suzanne C. Bart*

Cite This: *Inorg. Chem.* 2021, 60, 3460−3470 Read Online

ACCESS | Metrics & More | Article Recommendations | Supporting Information

ABSTRACT: Tellurium catecholate complexes were investigated to probe the redox chemistry of tellurium, whose oxidation state can span from −2 to +6. Treating TeO_2 with catechols resulted in tellurium coordination complexes in high yields within minutes to hours at room temperature or with extended heating, depending on the ligand substituents, giving Te(IV) complexes of the form $Te(\mathbf{C})_2$, where **C** = 3,5-di-*tert*-butylcatecholate, *o*-catecholate, or tetrachlorocatecholate. The redox behavior of these complexes was investigated through addition of organic oxidants, giving nearly quantitative adducts of pyridine *N*-oxide or *N*-methylmorpholine *N*-oxide with each tellurium complex, the latter set leading to ligand oxidation upon heating. Each compound was characterized crystallographically and computationally, providing data consistent with a mostly electrostatic interaction and very little covalent character between the *N*-oxide and Te complex. The Te *N*-oxide bond orders are consistently lower than those with the catechol derivatives, as characterized with the Mayer, Gopinathan−Jug (G-J), and first Nalewajski−Mrozek (N-M1) bond indices. The tellurium lone pair is energetically buried by 1.93−2.81 eV, correlating with the observation that the ligands are more reactive than the tellurium center toward oxidation. This combined experimental and theoretical study finds structure−property relationships between ligand design and reactivity that will aid in future efforts for the recovery of tellurium.

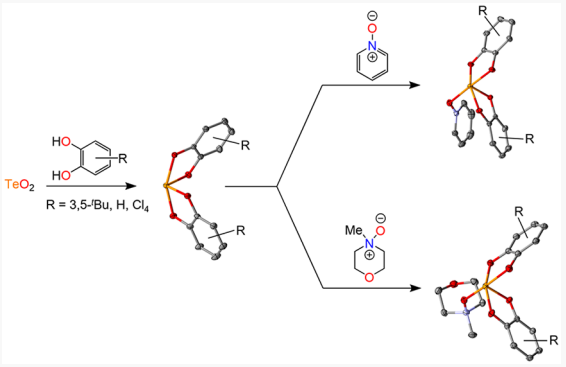

INTRODUCTION

Tellurium shares a curious place on the Periodic Table as one of the seven elements classified as a metalloid. These materials are aptly named, as they display properties of both metals and nonmetals and thus cannot rigidly be classified as either. Thus, the unusual properties of tellurium earned it the names *metallum problematicum* and *Aurum paradoxum*. Tellurium has a low Earth crustal abundance (0.002 ppm), similar to that of gold (0.004 ppm), making mining of this element cost ineffective.[1] Instead, this material is harvested from the anodic sludge byproduct of copper refining, requiring approximately 500 tons of copper ore to yield about 1 lb (0.45 kg) of tellurium.[2]

The low abundance of tellurium notwithstanding, it is now a major component of optoelectronic materials, with CdTe thin-film photovoltaics being chief among these. Commercialization of these devices represents an important step forward in the transition toward renewable energy but also an increasing chemical waste burden when these devices reach end of life. Therefore, the development of effective recycling and separation/extraction strategies for tellurium could offset current production needs and become a closed-cycle source of tellurium for device manufacturers.

Tellurium presents its own challenges for separations, as it exists in a variety of oxidation states, including −2, 0, +2, +4, and +6 (Chart 1). Previous work shows that the tellurium redox behavior is highly dependent on the ligand environment. For instance, recent results by Inagi and co-workers show unique redox behaviors of tellurophanes that differ from those of typical tellurium coordination compounds due to their π-extended structures.[3] Similarly, Gabbaï and co-workers have

Chart 1. Representative Examples and Formal Oxidation States of Some Common Tellurium Compounds

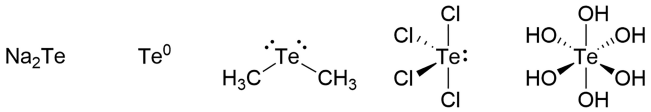

Received: January 14, 2021
Published: February 9, 2021

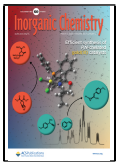

https://dx.doi.org/10.1021/acs.inorgchem.1c00126
Inorg. Chem. 2021, 60, 3460−3470

achieved the formation of telluronium ions, demonstrating that they are excellent σ-accepting ligands for transition metals.[4] This group has recently extended this chemistry to show that these telluronium(IV) cations can transport chloride anions across phospholipid bilayers more effectively than their neutral Te(II) precursors.[5]

This varied chemical behavior makes a judicious ligand choice for the intended application imperative, and this can be informed by understanding tellurium coordination chemistry and redox processes. Thus, redox-active ligands are attractive choices for this metalloid, as these ligands can accept or donate electrons into their π^* orbitals to modulate the electronics at metals. The *o*-catecholate/*o*-quinone family of ligands is particularly attractive for studying Te redox chemistry, as the members can exist in the catecholate (2−), semiquinone (1−), or quinone (0) ligand forms. Additionally, these ligands are sterically and electronically modular, commercially available, and inexpensive (Scheme 1), making them directly applicable

Scheme 1. Redox Behavior of Catecholate Ligands and Abbreviations for Substituted Catecholates and Quinones

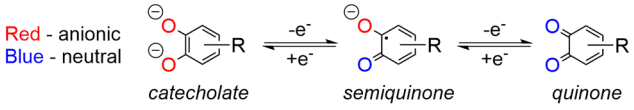

R=	abbrev.	abbrev.	abbrev.
3,5-di-*tert*-butyl	dtbc	dtbsq	dtbq
H	cat	sq	quin
tetrachloro	tcc	tcsq	tcq

to potential separation processes. Tellurium complexes employing *o*-catechols have been explored by Antikainen and Mälkönen, who showed that Te(*o*-catecholate)$_2$ was formed from the reductive condensation of Te(OH)$_6$ and *o*-catechol in only 0.5% yield.[6] Analogous reactions performed via potentiometric titrations, however, suggested a possible 3:1 catechol:telluric acid stoichiometry.[7] Other routes to Te(*o*-catecholate)$_2$ complexes were explored by Tuck, who showed that Te^0 could be oxidized by substituted *o*-quinones to give products in excellent yields.[8]

This catechol platform is especially desirable for studying oxidation chemistry, as it will be interesting to determine if electron loss occurs at the tellurium, to make a higher valent species, or at the ligand, to generate an oxidized form. The latter is well-precedented for redox-active ligand families, whereas the former tellurium chemistry is mainly restricted to Te(II/IV) and Te(IV/VI) couples.[9,10] Such examples include those from Seferos and co-workers, where tellurophanes were demonstrated to undergo reversible two-electron reductive elimination/oxidative addition of bromine.[11−13] Similarly, reversible two-electron oxidation of organoditelluride species was noted by Fujihara, Furukawa, and co-workers. In this case, two Te(II) centers were oxidized to Te(IV) centers using elemental chlorine and iodine, forming two Te−X centers and featuring a new Te−Te bond.[14,15] Also by two-electron oxidation, Gabbaï and co-workers have demonstrated oxygen atom transfer by treating a gold telluroether complex with H_2O_2, producing the tellurium(IV) terminal oxide complex.[16] The Gabbaï group has also demonstrated a more unusual transformation of a two-electron oxidation of a Te(III) center to a Te(V) center, utilizing both KF and methanol.[17]

Intrigued by this redox chemistry reported for tellurium, we sought to investigate if redox-active ligands could expand the possibilities for reactivity at tellurium centers. Herein, the synthesis and characterization of new tellurium catecholate coordination complexes are reported, as well as computational analyses to understand the electronic structures of these species. This combined experimental and computational study will help to predict future reactivity trends for applications toward tellurium recovery.

EXPERIMENTAL METHODS

General Considerations. All manipulations were carried out under an inert atmosphere of nitrogen or argon using either an MBraun glovebox or standard Schlenk line techniques, unless stated otherwise. Syntheses of **1** and **2** were carried out under ambient conditions. All chemicals were purchased from commercial sources and used as received, unless stated otherwise. When they were used under an inert atmosphere, toluene, THF, diethyl ether, and pentane were purified through a Seca solvent purification system[18] and stored over molecular sieves. Deuterated solvents were purchased from Cambridge Isotope Laboratories. Benzene-d_6 was dried over molecular sieves and sodium and degassed with three freeze−pump−thaw cycles. THF-d_8 was dried and stored over sodium. Pyridine-d_5 was dried over CaH_2 and degassed with three freeze−pump−thaw cycles. NMR spectra were recorded on Bruker AVANCE III 400 MHz and Bruker DRX 500 MHz spectrometers, and chemical shifts are referenced to residual solvent signals (^{1}H and ^{13}C) or an external standard (^{125}Te: 0.5 M Ph_2Te_2 in DCM-d_2, δ 422 ppm).[19] FT-IR spectra were recorded on a Thermo Nicolet 6700 spectrophotometer. Elemental analyses were performed by Midwest Microlab, LLC (Indianapolis, IN).

Synthesis of Te(dtbc)$_2$ (1). *Method A.* A solution of 3,5-di-*tert*-butylcatechol (2.032 g, 9.14 mmol) in 100 mL of toluene was added to a round-bottom flask containing TeO_2 (0.842 g, 5.28 mmol), TsOH (0.048 g, 5 mol %), and 2 g of Na_2SO_4. The reaction mixture quickly turned red, and dissolution of TeO_2 was complete within 30 min to give a red solution. This was filtered and evaporated to a thick red oil. The oil was dissolved in 100 mL of pentane and stirred rapidly overnight to precipitate **1** as a bright orange powder (1.783 g, 69%). Crystals of **1** were collected in similar yields by allowing a pentane solution to stand undisturbed for several days.

Method B. Te(OH)$_6$ (0.233 g, 1.01 mmol), 3,5-di-*tert*-butylcatechol (0.678 g, 3.05 mmol), and TsOH (0.009 g, 0.05 mmol) were combined in a round-bottom flask with 15 mL of toluene, and the mixture was refluxed overnight using a Dean−Stark apparatus. The resulting brown solution was evaporated to dryness and the remaining brown oil dissolved in 5 mL of pentane. Precipitation of orange crystals of **1** was accomplished after standing for several days (0.372 g, 65%). ^{1}H NMR (C_6D_6, 400 MHz): δ 7.06−6.96 (m, 4H), 1.51 (s, 11H), 1.47 (s, 7H), 1.21 (s, 7H), 1.18 (s, 11H). ^{13}C{^{1}H} NMR (C_6D_6, 101 MHz): δ 148.25, 147.87, 144.46, 143.76, 143.20, 143.07, 136.08, 115.05, 114.89, 110.45, 34.55, 34.15, 31.33, 29.32. ^{125}Te NMR (C_6D_6, 126 MHz): δ 1700.43, 1691.25.

Synthesis of Te(cat)$_2$ (2). Catechol (7.077 g, 64.3 mmol), TeO_2 (5.008 g, 31.4 mmol), and TsOH (0.295 g, 1.55 mmol) were placed in a round-bottom flask with 500 mL of toluene and stirred overnight at room temperature. The resulting slurry was filtered and washed sequentially with 100 mL each of toluene, ethanol, and pentane. Further purification was carried out using Soxhlet extraction into methanol. The extract was evaporated to dryness to give **2** as a bright yellow solid (7.98 g, 74%). ^{1}H NMR (THF-d_8, 400 MHz): δ 6.79−6.74 (m, 4H), 6.65−6.60 (m, 4H). ^{13}C{^{1}H} NMR (THF-d_8, 101 MHz): δ 149.10, 123.46, 115.41. ^{125}Te NMR (THF-d_8, 126 MHz): δ 1680.58.

Synthesis of Te(tcc)$_2$·*n*THF (3). *Method A.* TeO_2 (0.202 g, 1.27 mmol), tetrachlorocatechol (0.620 g, 2.50 mmol), TsOH (0.012 g, 5 mol %), and 1 g of Na_2SO_4 were placed in a Schlenk flask, a reflux condenser was attached, and the system was purged with argon. Dry

https://dx.doi.org/10.1021/acs.inorgchem.1c00126
Inorg. Chem. 2021, 60, 3460−3470

toluene was added via cannula and the reaction mixture refluxed for 4 days. The resulting yellow slurry was evaporated to dryness and extracted into 20 mL of dry THF. The filtrate was dried under vacuum and washed with toluene (3 × 10 mL) to remove residual catechol and coordinated THF. The residue was dried under vacuum to give **3** as a yellow solid (0.323 g, 42%).

Method B. **3** was synthesized by the procedure in ref 8 and isolated as a THF solvate by extraction into THF and evaporation of the filtrate under vacuum. The degree of solvation was quantified through ^{1}H NMR and elemental analysis for *n*THF, *n* = 1.58. ^{13}C{^{1}H} NMR (THF-d_8, 126 MHz): δ 146.27, 123.17, 119.32. ^{125}Te NMR (THF-d_8, 158 MHz): δ 1684.49. Anal. Calcd for $C_{12}Cl_8O_4Te{\cdot}1.58C_4H_8O$: C, 30.01; H, 1.74. Found: C, 29.89; H, 1.82.

Synthesis of Te(dtbc)$_2$PyNO (4). A solution of pyridine *N*-oxide (0.117 g, 1.23 mmol) in 10 mL of toluene was placed in a scintillation vial containing a solution of **1** (0.697 g, 1.23 mmol) in 10 mL of toluene and stirred at room temperature for 90 min. Afterward the mixture was evaporated to dryness and triturated with pentane (3 × 5 mL) to give **4** as a pale yellow solid (0.789 g, 97%). ^{1}H NMR (C_6D_6, 400 MHz): δ 7.73 (d, *J* = 6.14 Hz, 2H), 7.09−6.76 (m, 4H), 6.20 (t, *J* = 7.59 Hz, 1H), 6.03 (t, *J* = 7.07 Hz, 2H), 1.49 (s, 10H), 1.34−1.14 (m, 26H). ^{13}C{^{1}H} NMR (C_6D_6, 101 MHz): δ 149.54, 145.37, 142.03, 140.52, 135.79, 130.61, 125.63, 114.10, 113.91, 110.68, 110.45, 35.03, 34.85, 34.53, 31.96, 29.91, 29.83. ^{125}Te NMR (C_6D_6, 126 MHz): δ 1594.46, 1586.96. Anal. Calcd for $C_{33}H_{45}NO_5Te$: C, 59.75; H, 6.84; N, 2.11. Found: C, 59.57; H, 6.64; N, 2.21.

Synthesis of Te(cat)$_2$PyNO (5). Pyridine *N*-oxide (0.094 g, 0.99 mmol) and **2** (0.343 g, 1.00 mmol) were placed in a round-bottom flask along with 20 mL of THF and stirred at room temperature for 1 h. The resulting slurry was evaporated to dryness and triturated with 3 mL of pentane to give **5** as an off-white solid (0.443 g, quantitative). ^{1}H NMR (THF-d_8, 400 MHz): δ 8.34 (d, *J* = 6.51 Hz, 2H), 7.60 (t, *J* = 7.65 Hz, 1H), 7.47 (t, *J* = 7.03 Hz, 2H), 6.63−6.56 (m, 4H), 6.56−6.48 (m, 4H). ^{13}C{^{1}H} NMR (THF-d_8, 101 MHz): δ 150.39, 141.85, 131.75, 127.23, 120.35, 115.01. ^{125}Te NMR (THF-d_8, 126 MHz): δ 1606.50. Anal. Calcd for $C_{17}H_{13}NO_5Te$: C, 46.52; H, 2.99; N, 3.19. Found: C, 46.51; H, 3.01; N, 3.24.

Synthesis of Te(tcc)$_2$PyNO·THF (6). A solution of **3** (0.987 g, *n*THF = 1.58, 1.35 mmol) in 15 mL of THF was placed in a round-bottom flask containing a solution of pyridine *N*-oxide (0.128 g, 1.35 mmol) in 5 mL of THF and stirred at room temperature for 1 h. The resulting solution was evaporated to give **6** as a faint yellow solid (1.035 g, 97%). ^{1}H NMR (THF-d_8, 400 MHz): δ 8.63 (d, *J* = 6.24 Hz, 2H), 8.00 (t, *J* = 7.33 Hz, 1 H), 7.76 (t, *J* = 6.81 Hz, 2H), 3.62 (m, 4H) 1.77 (m, 4H). ^{13}C{^{1}H} NMR (THF-d_8, 101 MHz): δ 147.71, 142.96, 137.51, 128.16, 122.73, 118.76, 68.39, 26.55. ^{125}Te NMR (THF-d_8, 126 MHz): δ 1547.91. Anal. Calcd for $C_{17}H_5Cl_8NO_5Te{\cdot}C_4H_8O$: C, 32.07; H, 1.67; N, 1.78. Found: C, 32.57; H, 1.83; N, 1.62.

Synthesis of Te(dtbc)$_2$NMMO (7). A solution of **1** (0.553 g, 0.973 mmol) in 20 mL of toluene was placed in a round-bottom flask containing *N*-methylmorpholine *N*-oxide (0.114 g, 0.973 mmol), and the suspension was stirred at room temperature for 1 h. A small amount of precipitate was removed by filtration, the filtrate was reduced to dryness under vacuum and washed with pentane (3 × 10 mL), and the residual volatiles were removed under vacuum to give **7** as an off-white solid (0.610 g, 92%). ^{1}H NMR (C_6D_6, 400 MHz): δ 7.11 (d, *J* = 2.20 Hz, 1H), 7.00 (d, *J* = 2.23 Hz, 1H), 6.97 (d, *J* = 2.17 Hz, 1H), 6.95 (d, *J* = 2.26 Hz, 1H), 4.07 (ddd, *J* = 13.06, 11.37, 1.96 Hz, 2H), 3.06 (dd, *J* = 12.63, 3.48 Hz, 2H), 2.68 (d, *J* = 11.53 Hz, 2H), 2.47 (s, 3H), 1.88 (td, 11.64, 3.68 Hz, 2H), 1.57 (s, 10H), 1.43 (s, 8H), 1.32 (s, 8H), 1.26 (s, 10H). ^{13}C{^{1}H} NMR (C_6D_6, 101 MHz): δ 150.61, 149.56, 145.93, 145.22, 142.29, 141.65, 136.00, 135.72, 129.34, 125.70, 114.08, 113.86, 110.74, 110.37, 64.65, 61.34, 58.54, 35.11, 34.94, 34.62, 34.56, 32.07, 32.03, 30.08, 30.03. ^{125}Te NMR (C_6D_6, 126 MHz): δ 1558.50, 1550.95. Anal. Calcd for $C_{33}H_{51}NO_6Te$: C, 57.83; H, 7.50; N, 2.04. Found: C, 57.50; H, 7.79; N, 2.35.

Synthesis of Te(cat)$_2$NMMO (8). *N*-Methylmorpholine *N*-oxide (0.159 g, 1.36 mmol) and **2** (0.462 g, 1.34 mmol) were placed in a round-bottom flask along with 20 mL of THF and stirred at room temperature for 1 h. The resulting solution was evaporated to a sticky solid and triturated with pentane (3 × 3 mL) to give **6** as a pale yellow solid (0.634 g, quantitative). ^{1}H NMR (THF-d_8, 400 MHz): δ 6.69−6.65 (m, 4H), 6.57−6.53 (m, 4H), 4.26 (ddd, *J* = 12.55, 11.22, 2.15 Hz, 2H), 3.68 (dd, *J* = 12.83, 3.86 Hz, 2H), 3.50 (d, *J* = 11.76 Hz, 2H), 3.36 (td, *J* = 11.68, 3.71 Hz, 2H), 3.31 (s, 3H). ^{13}C{^{1}H} NMR (THF-d_8, 101 MHz): δ 152.01, 121.98, 113.25, 66.17, 62.51, 58.74. ^{125}Te NMR (THF-d_8, 126 MHz): δ 1596.36. Anal. Calcd for $C_{17}H_{19}NO_6Te$: C, 44.30; H, 4.15; N, 3.04. Found: C, 44.31; H, 3.96; N, 2.75.

Synthesis of Te(tcc)$_2$NMMO (9). A solution of **3** (1.327 g, *n*THF = 1.58, 1.81 mmol) in 20 mL of THF was placed in a round-bottom flask containing *N*-methylmorpholine *N*-oxide (0.212 g, 1.81 mmol), and the resulting amber solution was stirred for an additional 1 h at room temperature. The solution was evaporated to dryness to give **9** as an off-white solid (1.341 g, quantitative). ^{1}H NMR (THF-d_8, 400 MHz): δ 4.32 (t, *J* = 11.67 Hz, 2H), 3.87 (d, *J* = 12.73 Hz, 2H), 3.68 (d, *J* = 11.38 Hz, 2H), 3.57 (obscured by residual solvent signal), 3.43 (s, 3H), 1.78 (m, nH). ^{13}C{^{1}H} NMR (THF-d_8, 101 MHz): δ 146.42, 121.38, 117.55, 67.13, 65.28, 61.34, 58.09, 25.30. ^{125}Te NMR (THF-d_8, 126 MHz): δ 1565.91. Anal. Calcd for $C_{17}H_{11}Cl_8NO_6Te$: C, 27.72; H, 1.51; N, 1.90. Found: C, 28.05; H, 1.58; N, 1.91.

Computational Methods. Initial molecular structures were taken as obtained from the single-crystal structures determined by X-ray diffraction and optimized with quantum mechanics using density functional theory (DFT) in the Amsterdam Density Functional (ADF) 2018 program.[20] The hybrid-generalized gradient approximation (GGA) Becke three-parameter Lee−Yang−Parr (B3LYP) functional[21,22] and a Slater-type[23] triple-ζ basis set with one polarization function[23] (TZP) were used for the optimizations; large atomic cores were frozen, and the Becke grid was set to *very good*.[24] Scalar relativistic corrections were applied with the zero-order regular approximation (ZORA) formalism as implemented in the ZORA basis sets in ADF, using the default minimum of neutral atomic potential approximation (MAPA) potential.[25] The self-consistent field (SCF) convergence was set to 1.0e^{-6}. This level of theory was applied to all calculations, including the frontier molecular orbitals and Te symmetry combinations of fragment orbital (SFO) contributions, numerical frequencies, electrostatic maps, atomic charges, and bond order analysis. The structures and isosurfaces (0.03) were visualized with the ADF graphic user interface (GUI) ADFView. The bond order analysis included the formalisms by Mayer,[26] Gopinathan−Jug[27] (G-J), and the first variant of Nalewajski−Mrozek[28,29] (N-M) as implemented in ADF.

RESULTS AND DISCUSSION

The starting point of this chemistry was to examine reactions using common sources of tellurium, including Te^0 metal, TeO_2, and $Te(OH)_6$. Ligand metalation was first attempted using dtbc (dtbc = 3,5-di-*tert*-butylcatechol), as this was precedented in the literature.[8] Furthermore, its electron-donating *tert*-butyl substituents should facilitate metalation. Repeating this literature procedure, by stirring dtbq (dtbq = 3,5-di-*tert*-butylquinone) with Te^0, produced the expected product, $Te(dtbc)_2$, in 85% yield (**1**, Scheme 2a). Following this, a revised method was attempted on the basis of hexavalent telluric acid, $Te(OH)_6$. Treating $Te(OH)_6$ with dtbc in toluene resulted in the consumption of insoluble $Te(OH)_6$ after 16 h at reflux with catalytic TsOH and using a Dean−Stark trap to remove water (Scheme 2b). Following workup, orange crystals precipitated from pentane over a few days in 65% yield.

The most convenient synthesis of **1**, however, was accomplished using Te(IV). Reactions involving common Te(IV) materials were investigated because reactions of TeO_2 with glycols have been established in the literature.[30] TeO_2 is

https://dx.doi.org/10.1021/acs.inorgchem.1c00126
Inorg. Chem. 2021, 60, 3460−3470

Scheme 2. Synthesis of 1

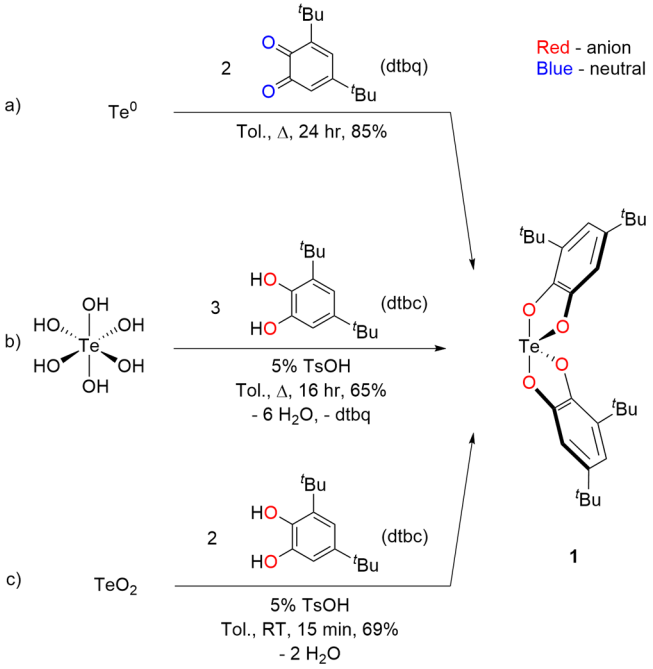

also attractive, given that it is a common Te-containing compound produced in current device recycling strategies.[31] Treating TeO_2 and stoichiometric quantities of dtbc in toluene with catalytic TsOH resulted in the complete consumption of TeO_2 within 30 min at room temperature. Evaporation of this solution resulted in a red-orange oil, and **1** precipitated from pentane solution in 69% yield (Scheme 2c).

With this success, metalation of the unsubstituted catechol was first attempted by treating Te^0 with unsubstituted *o*-quinone. This reaction did not work well, however. The majority of Te^0 remained unreacted after stirring for 3 days at RT, with only a trace of a Te-bearing product detected in the organic layer. This was likely complicated by the instability of the free quinone. It was previously reported that freshly prepared solutions are suitable for synthesis for a few hours at room temperature,[32] but the reaction with Te^0 appears to require higher temperatures or longer reaction times not amenable to this method.

Metalation of the parent catechol, *o*-catechol, was also not successful using higher-valent starting materials. Previously, a tellurium-containing product was synthesized in trace quantities via the condensation of *o*-catechol with $Te(OH)_6$ in water, along with sacrificial oxidation of 1 equiv of catechol.[6] The most efficient procedure for the unsubstituted catechol metalation was to instead stir with TeO_2 for 16 h at room temperature (eq 1); however, this product had negligible solubility in toluene. In fact, this product was only sparingly soluble in noncoordinating solvents. The pure product was obtained in good yield via Soxhlet extraction with MeOH and assigned as $Te(cat)_2$ (**2**). Although the compound is moderately sensitive to hydrolysis, single crystals were grown from slow evaporation in MeOH.

The case of the tetrachlorocatecholate is the most difficult for metalation, given the highly electron withdrawing nature of this ligand; however, oxidation of Te^0 using tetrachloroquinone is very efficient. In this case, a literature procedure was used and modified.[8] Stirring tetrachloroquinone with Te metal

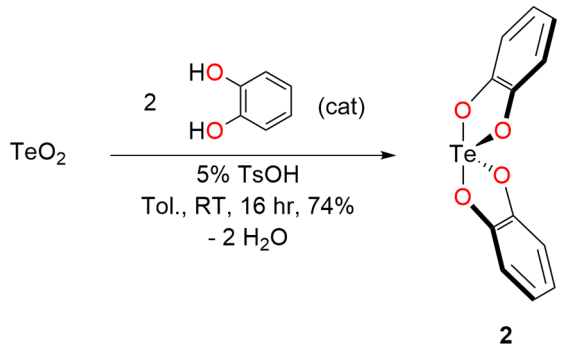

gave the desired product, $Te(tcc)_2$ (**3**), with an additional purification step to remove any residual Te^0 or advantageous TeO_2 impurity (Scheme 3a). This product can also be

Scheme 3. Synthesis of 3

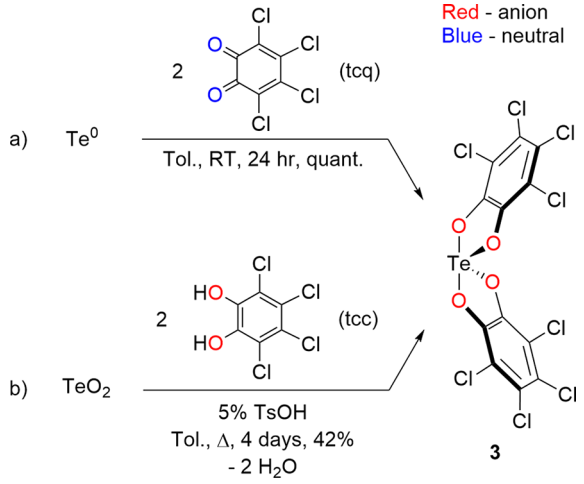

generated as a major component by refluxing TeO_2 and tetrachlorocatecholate in toluene for 4 days, but this synthesis is not as high-yielding as that with Te^0 (Scheme 3b). Using $Te(OH)_6$ did not give tractable products with the tetrachlorocatecholate ligand.

X-ray crystallography was used to determine the molecular structures of **1**−**3**. Given that redox-active ligands are used, this is also a convenient probe for oxidation state changes by an analysis of ligand metrical parameters (Table 1 and Figure 1). Single crystals of **1**−**3** were grown using the following methods, respectively: concentrated pentane solution at 4 °C, slow evaporation from methanol, and concentrated THF solution at −35 °C.

As shown in Figure 1, **1**−**3** share a seesaw geometry consistent with a 10-Te-4 hypervalent structure.[33] It should be noted that **2** is consistent with a previously reported structure, though it is reported herein with much greater precision, as required for a complete comparison among the family of compounds.[34] For the series of complexes **1**−**3**, each catecholate ligand occupies both one equatorial position and one axial position, giving separate Te−O geometric parameters due to the difference in 2c-2e and 3c-4e bonding, respectively. The set of $Te-O_{eq}$ distances (**1**, 1.952(1), 1.952(1) Å; **2**, 1.956(2), 1.966(1) Å; **3**, 1.968(1), 1.988(1) Å) are nearly identical within each structure (less so in **3** potentially due to THF coordinated trans to O_{eq}) and trend toward a longer $Te-O_{eq}$ distance with less electron donating catecholate ligands.

https://dx.doi.org/10.1021/acs.inorgchem.1c00126
Inorg. Chem. 2021, 60, 3460−3470

Table 1. Selected Bond Metrics for 1−3[a]

	Te(dtbc)$_2$ (**1**)	Te(cat)$_2$ (**2**)	Te(tcc)$_2$·3THF (**3**)
Te−O$_{ax}$	2.042(1)	2.092(1)	2.042(1)
Te−O$_{ax}$′	2.008(1)	2.024(1)	2.077(1)
Te−O$_{eq}$	1.952(1)	1.956(2)	1.968(1)
Te−O$_{eq}$′	1.952(1)	1.966(1)	1.988(1)
C−O$_{ax}$	1.356(3)	1.370(2)	1.339(2)
C−O$_{ax}$′	1.375(2)	1.369(2)	1.339(2)
C−O$_{eq}$	1.377(2)	1.382(2)	1.362(2)
C−O$_{eq}$′	1.390(2)	1.379(2)	1.356(2)
O$_{ax}$−Te−O$_{ax}$′	158.08(5)	154.00(5)	152.52(5)
O$_{eq}$−Te−O$_{eq}$′	94.55(5)	96.45(5)	94.18(5)
O$_{ax}$−Te−O$_{eq}$	80.96(5)	80.78(5)	81.56(5)
O$_{ax}$′−Te−O$_{eq}$′	81.84(5)	81.55(5)	78.79(5)

[a]Bonds are given in Angstroms (Å), and angles are given in degrees (°).

The set of Te−O$_{ax}$ distances (**1**, 2.042(1), 2.008(1) Å; **2**, 2.092(1), 2.024(1) Å; **3**, 2.042(1), 2.077(1) Å) show more variability within each structure, though the average Te−O$_{ax}$ distance follows the same trend as with Te−O$_{eq}$ with respect to the electron-donating strength of the catecholate ligand. The O$_{ax}$−Te−O$_{ax}$′ angle is significantly distorted from 180° (**1**, 158.08(5)°; **2**, 154.00(5)°; **3**, 152.52(5)°), though this is consistent across each structure. The O$_{eq}$−Te−O$_{eq}$′ angle shows less distortion from 90° (**1**, 94.55(5)°; **2**, 96.45(5)°; **3**, 94.18(5)°). The geometry of the catecholate ligands is unremarkable, though special attention should be paid to the C−O distances as a metric for the ligand oxidation state. The trend toward shorter C−O distances from **1** to **3** is comparable to a set of structurally similar Ge complexes and their respective C−O distances: [Ge(OH)(dtbc)$_2$][Et$_3$NH], 1.36(1), 1.36(1), 1.37(1), 1.38(1) Å; [GeMe(cat)$_2$][Et$_4$N], 1.343(9), 1.343(9), 1.367(9), 1.367(9) Å; [GeMe(tcc)$_2$]-[Et$_4$N], 1.328(6), 1.337(6), 1.339(6), 1.340(6) Å.[35,36] The C−O distances for **1**−**3**, consistent with the catecholato structures, are significantly longer than those observed in unbound quinones: 3,5-di-*tert*-butyl-*o*-quinone, 1.223(2), 1.221(3) Å; *o*-quinone, 1.220 Å; tetrachloroquinone, 1.208(4) Å.[37−39] It should be noted that the orientations of the 3,5-di-*tert*-butylcatecholate ligands in **1** give rise to three potential isomers (or two if the compound is considered as a square pyramid), as has been previously discussed and observed in solution as two sets of NMR resonances.[8] On the basis of the structural characterization of **1** and adducts of **1**, as discussed later, all three isomers are shown to be present in some fashion, likely through a low-lying pseudorotation or chemical exchange of ligands in solution.

In order to probe where oxidation occurs in complexes **1**−**3**, the Te(IV) center or the catecholate ligands, their reactivity with chemical oxidants was explored. Common organic oxidants, including pyridine *N*-oxide (PyNO) and *N*-methylmorpholine *N*-oxide (NMMO), were chosen, as shown in Scheme 4. Addition of PyNO to **1** in toluene or

Scheme 4. Synthesis of 4−9

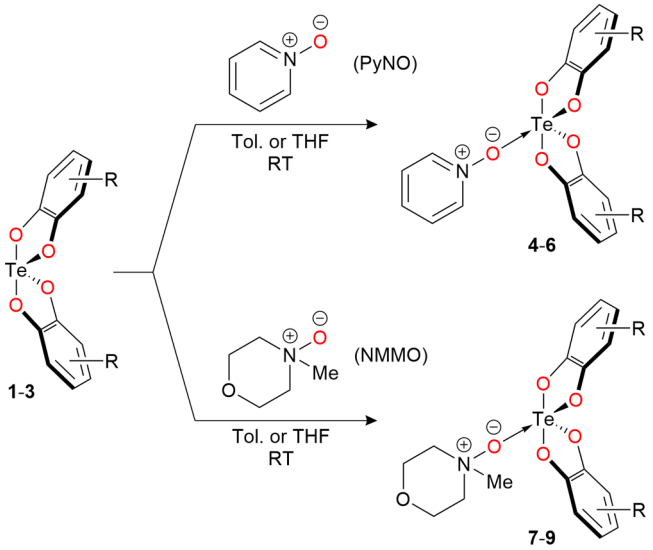

R = 3,5-di-*tert*-butyl (**1**, **4**, **7**), H (**2**, **5**, **8**), or tetrachloro (**3**, **6**, **9**)

benzene produced an immediate change in the red-orange color to yellow. Analysis of this reaction by NMR spectroscopy revealed a single product in both the ^{1}H and ^{125}Te spectra, providing data consistent with the formation of a 1:1 adduct, **4**, and not an oxidation or O-atom transfer reaction. Heating this solution to 80 °C for 5 days and watching for the products of the latter reactions only revealed the high thermal stability of **4**. ^{125}Te NMR spectroscopy is particularly useful in this regard, owing to its wide spectral window and chemical shifts being highly susceptible to changes in the coordination environment. Therefore, the observation that reactions of **1**−**3** with *N*-oxides only resulted in a ca. 100 ppm upfield shift was not consistent with any significant change in the bonding about Te or a change in oxidation state. A similar degree of change in the ^{125}Te resonance was previously observed for 1:1 adducts of **1** with bipyridine or BCl$_3$.[8]

Addition of NMMO to **1** in toluene or benzene resulted in a similar rapid shift to a yellow solution, in conjunction with the

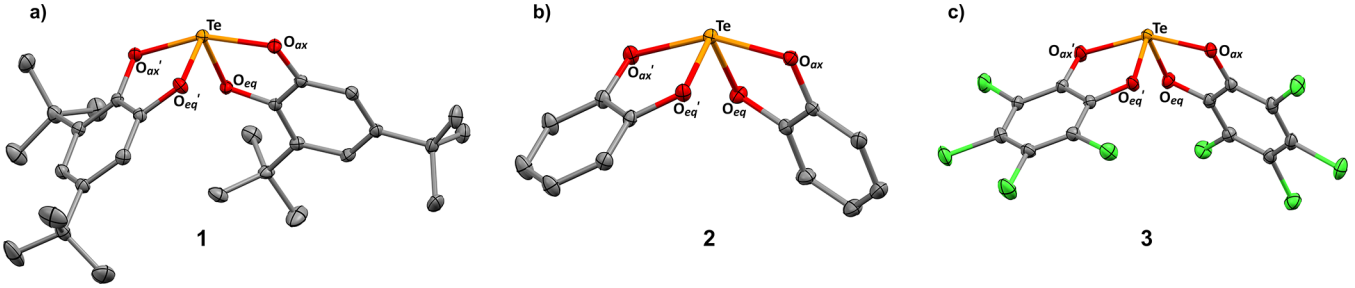

Figure 1. ORTEP diagrams of **1**−**3** shown with 50% probability ellipsoids: (a) Te(dtbc)$_2$ (**1**); (b) Te(cat)$_2$ (**2**); (c) Te(tcc)$_2$ (**3**), with the three coordinated THF molecules omitted for clarity. Hydrogen atoms and cocrystallized solvent molecules have been omitted for clarity.

https://dx.doi.org/10.1021/acs.inorgchem.1c00126
Inorg. Chem. 2021, 60, 3460−3470

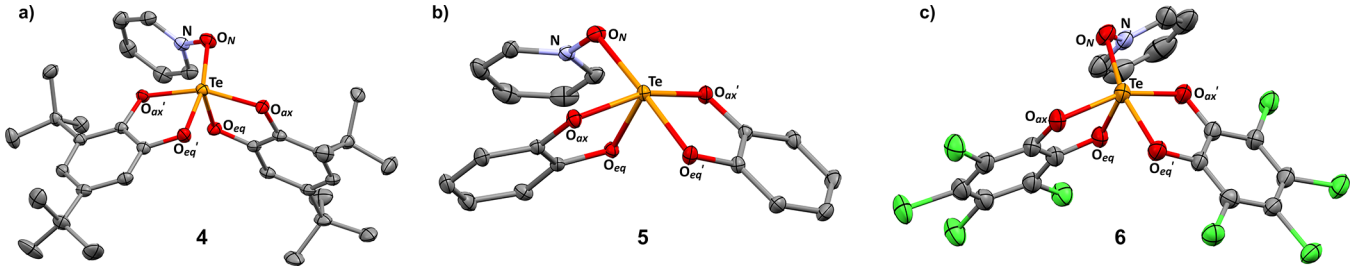

Figure 2. ORTEP diagrams of **4**–**6** shown with 50% probability ellipsoids: (a) $Te(dtbc)_2$·PyNO (**4**); (b) $Te(cat)_2$·PyNO (**5**); (c) $Te(tcc)_2$·PyNO (**6**), with the coordinated THF molecule omitted for clarity. Hydrogen atoms and cocrystallized solvent molecules have been omitted for clarity.

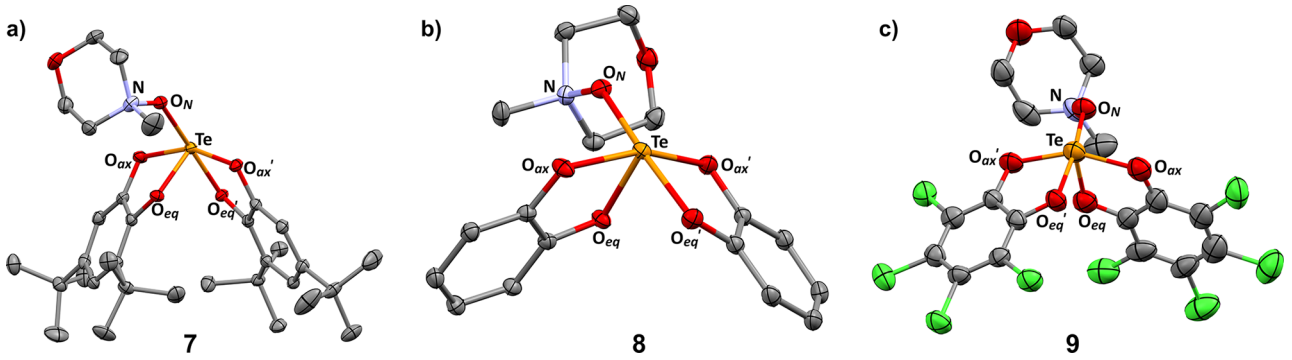

Figure 3. ORTEP diagrams of **7**–**9** shown with 50% probability ellipsoids: (a) $Te(dtbc)_2$·NMMO (**7**); (b) $Te(cat)_2$·NMMO (**8**); (c) $Te(tcc)_2$·NMMO (**9**), with the second independent moiety omitted for clarity. Hydrogen atoms and cocrystallized solvent molecules have been omitted for clarity.

Table 2. Selected Bond Metrics for 4–9[a]

	$Te(dtbc)_2$·PyNO (**4**)	$Te(cat)_2$·PyNO (**5**)	$Te(tcc)_2$·PyNO (**6**)	$Te(dtbc)_2$·NMMO (**7**)	$Te(cat)_2$·NMMO (**8**)	$Te(tcc)_2$·NMMO (**9**)
Te–O_{ax}	2.054(1)	2.084(1)	2.116(3)	2.047(2)	2.1052(9)	2.069(5)
Te–O_{ax}'	2.030(1)	2.036(1)	2.045(3)	2.037(2)	2.024(1)	2.015(4)
Te–O_{eq}	1.955(2)	1.984(2)	1.981(3)	1.993(2)	1.9844(8)	1.979(5)
Te–O_{eq}'	1.981(1)	2.013(1)	2.034(3)	2.002(2)	2.041(1)	2.037(4)
Te–O_N	2.397(2)	2.274(1)	2.333(3)	2.214(2)	2.1869(8)	2.165(4)
O_N–N	1.339(2)	1.351(2)	1.335(5)	1.413(3)	1.418(1)	1.441(6)
C–O_{ax}	1.367(2)	1.360(2)	1.344(5)	1.360(3)	1.347(1)	1.337(9)
C–O_{ax}'	1.375(2)	1.358(2)	1.342(5)	1.367(3)	1.357(1)	1.349(6)
C–O_{eq}	1.380(2)	1.372(2)	1.366(5)	1.383(3)	1.364(1)	1.368(8)
C–O_{eq}'	1.374(2)	1.370(2)	1.357(5)	1.377(3)	1.367(1)	1.361(7)
O_{ax}–Te-O_{ax}'	158.47(6)	158.93(6)	156.4(1)	156.84(8)	159.18(4)	156.0(2)
O_{eq}–Te-O_{eq}'	92.80(6)	87.38(6)	88.2(1)	87.20(7)	86.22(4)	86.1(2)
O_{ax}–Te–O_{eq}	80.54(6)	79.26(5)	78.93(1)	79.16(7)	78.85(3)	79.4(2)
O_{ax}'–Te–O_{eq}'	81.33(5)	82.07(6)	80.3(1)	81.02(7)	80.60(4)	80.1(2)
O_N–Te–O_{eq}	80.59(5)	81.55(5)	81.4(1)	86.58(7)	85.90(3)	85.2(2)
O_N–Te–O_{eq}'	164.06(5)	165.72(6)	155.8(1)	169.16(7)	163.61(4)	166.9(2)
O_N–Te–O_{ax}	107.16(5)	95.89(5)	111.2(1)	101.78(7)	100.01(3)	102.5(2)
N–O_N–Te	119.4(1)	121.9(1)	119.7(2)	139.3(2)	136.72(6)	138.2(3)

[a]Bonds are given in angstroms (Å), and angles are given in degrees (deg).

complete dissolution of NMMO, suggesting a similar adduct, **7**, had formed. ^1H and ^{125}Te NMR spectra confirmed this hypothesis, showing no signs of oxidation or O-atom transfer reaction. However, heating **7** at 80 °C resulted in a secondary reaction, consistent with the oxidation of catecholate to quinone and release of *N*-methylmorpholine, presumably forming TeO_2 from an O-atom transfer reaction, though this could not be detected by solution NMR spectroscopy. Single crystals of compounds **4** and **7** grown by slow evaporation from benzene confirmed the formation of both products.

Addition of iodosylbenzene (PhIO) to **1** in benzene or toluene did not result in any detectable adduct formation; only the slow formation of dtbq was observed coinciding with the slow dissolution of PhIO. The analogous set of reactions with **2** and **3** also did not give the desired adduct. Given that PyNO was not oxidizing enough to observe oxidation of **1**–**3**, even under forcing conditions, and similarly that PhIO was too oxidizing for **1**–**3** to observe the intermediate adduct formation, the reaction of **1**-**3** with NMMO was examined in greater detail in order to ascertain what effect a change in ligand substitution had made. Solutions of **7**–**9** in THF-d_8

https://dx.doi.org/10.1021/acs.inorgchem.1c00126
Inorg. Chem. 2021, 60, 3460–3470

were heated at 80 °C and monitored by ^{1}H NMR spectroscopy over the course of 24 h. While the formation of 3,5-di-*tert*-butylquinone was observed upon heating **7**, observation of the unstable *o*-quinone and ^{1}H NMR silent tetrachloroquinone proved elusive when **8** and **9** were heated, respectively. Instead, the decrease in ^{1}H NMR spectroscopic signals associated with bound NMMO was analyzed. From this, **7** reacts at a significantly faster rate in comparison to either **8** or **9**, owing to the lower oxidation potential of the electron-rich catecholate ligands in **7** (Figure S31). To confirm that loss of NMMO was not due to thermal decomposition of solely the *N*-oxide ligand, a control reaction of NMMO dissolved in MeCN-d_3 was studied under the same conditions. Previous reports cited no observed decomposition at 60 °C,[40] and our findings at 80 °C were in line with this, giving less than 5% conversion of NMMO to *N*-methylmorpholine after 22 h (in comparison to approximately 50% loss of NMMO when **8** or **9** was heated).

Single crystals of compounds **4** and **7** were grown by slow evaporation from benzene, compound **5** from THF at −35 °C, and compounds **6**, **8**, and **9** by vapor diffusion of toluene into THF at −35 °C. As shown in Figures 2 and 3, compounds **4**−**9** feature the same structural characteristic, where a single new *N*-oxide ligand is bound in a *trans* orientation to one of the Te−O_{eq} bonds (for consistency, labeling follows that O_N is always *trans* to O_{eq}'), establishing a new pseudo-square-pyramidal geometry around the Te center. The most useful structural characteristics to gauge the strength of interactions present are the N−O_N and Te−O_N distances. If the *N*-oxide ligand is actively participating in 3c-4e bonding with Te and O_{eq}', a resulting lengthening of the Te−O_{eq}' distance should also be observable. Furthermore, if the equilibrium geometry lies toward the side of O-atom transfer and catecholate oxidation, a noticeable retraction of the C−O distance should be observed. As shown in Table 2, the N−O_N distances for complexes **4**−**6** were found to be 1.339(2), 1.351(2), and 1.335(5) Å, respectively, which is consistent with the N−O distance of 1.330 Å within the free ligand.[41] The Te−O_N distances in complexes **4**−**6** were found to be 2.397(2), 2.274(1), and 2.333(3) Å, respectively. Compound **5** shares both the longest N−O_N and shortest Te−O_N distances, suggesting a stronger interaction; however, compound **5** is constructed from the least sterically encumbered parent complex. To further probe if this variation is driven by a stronger interaction or simply through sterics or crystal-packing forces, the change in Te−O_{eq}' distance was examined. The differences in Te−O_{eq}' distances between compounds **1**−**3** (average: **1**, 1.952(1) Å; **2**, 1.961(2) Å; **3**, 1.978(1) Å) and **4**−**6** (**4**, 1.981(1) Å; **5**, 2.013(1) Å; **6**, 2.034(3) Å) are respectively +0.029, +0.052, and +0.056 Å. This suggests similar Te−O_N interactions in **5** and **6**, despite the observed structural differences about the *N*-oxide.

As shown in Table 2, compounds **7**−**9** feature N−O_N distances of 1.413(3), 1.418(1), and 1.441(6) Å, respectively, comparatively longer than 1.391 Å for free *N*-methylmorpholine *N*-oxide.[42] Te−O_N distances for **7**−**9** were found to be 2.214(2), 2.1869(8), and 2.165(4) Å, respectively. The trend toward longer N−O_N and shorter Te−O_N distances follows what should be expected for **7**−**9**, where an increasing electron-withdrawing character of the catecholate ligands results in an increasingly positive charge on the Te center. Presumably, the lack of N═O character in NMMO, given by the longer N−O_N distance and lower energy N−O stretching mode, enhances the electrostatic Te−O_N interaction more than was observed in **4**−**6**. On examination of the C−O distances in **4**−**6** in comparison to **1**−**3**, very little shortening is observed that would be indicative of ligand oxidation. The average C−O_{ax} and C−O_{eq} distances show that the set of C−O distances associated with **1**, **4**, and **7** and **3**, **6**, and **9** are independent of which oxidant is coordinated to Te. The set of C−O distances in **2**, **5**, and **8** do show a slight shortening as stronger oxidants are bound to Te; however, the shortest distance is still >0.1 Å from the C═O distance observed in the parent *o*-quinone (1.220 Å).[38]

Compounds **1**−**9** were further studied using IR spectroscopy to probe the new Te−O_N interaction, as this method is less affected by steric repulsion or crystal-packing forces that may interfere with direct correlation of the measured Te−O_N distance and the strength of the interaction (Figure 4). The

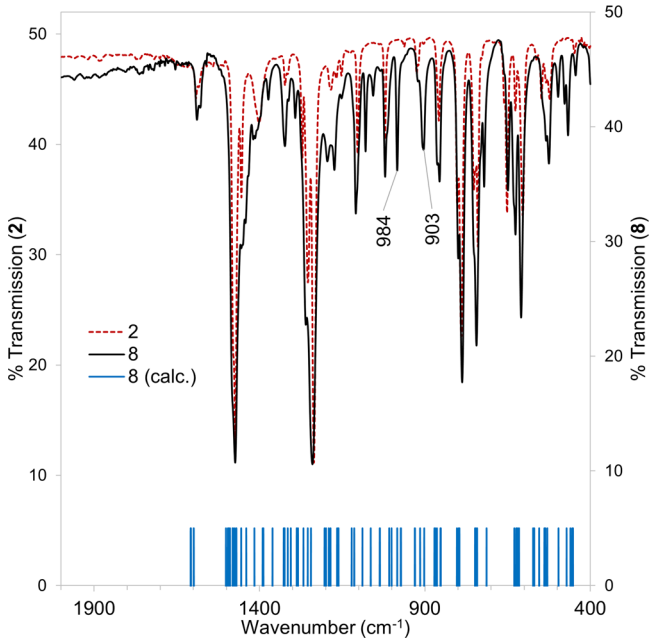

Figure 4. FT-IR spectra (KBr) of **2** (red) and **8** (black). Calculated wavenumbers for vibrational modes are **8** included for comparison (blue).

N−O stretching mode is sensitive to electron donation from the oxygen atom to tellurium, resulting in lowering of the N−O vibrational frequency. This has been studied on similar complexes such as PyNO adducts of zirconyl, thorium, and uranyl perchlorates, PyNO adducts of transition-metal perchlorates (M = Cr, Mn, Fe, Co, Ni, Cu, Zn, Al), and NMMO adducts of La, Nd, and Eu picrates.[43−45] Compounds **1**−**3** all feature a strong absorbance near 1240−1245 cm^{-1} which could potentially mask the N−O stretching mode in PyNO. The vibrational spectra of **4**−**6**, however, feature new, strong absorbances shifted approximately 40 cm^{-1} toward lower energy vs free PyNO, as shown in Table 3. This weakening of the N−O stretching mode was consistent with earlier studies also showing a 40−60 cm^{-1} shift toward lower energy.[43,44] Across the series, however, **4** and **5** share nearly identical N−O stretching frequencies, with **6** showing a slightly lower energy vibration. This was confirmed through an analysis of calculated vibrational modes with DFT, pointing toward **6** as containing a noticeably weaker N−O stretch. NMMO features two N−O stretching modes as discussed previously,[46] and the spectra of **7**−**9** show that the lower energy N−O

https://dx.doi.org/10.1021/acs.inorgchem.1c00126
Inorg. Chem. 2021, 60, 3460−3470

Table 3. N−O Stretching Frequencies for Pyridine *N*-Oxide Adducts 4−6

	ν_{NO} (cm^{-1})	
compound	exptl	calcd
PyNO	1244	1318
4	1201	1243, 1245
5	1198	1240
6	1178−1202	1192, 1225

stretch has been weakened by ca. 30 cm^{-1} (Table 4). This was consistent with the reported lanthanide NMMO complexes

Table 4. N−O Stretching Frequencies for *N*-Methylmorpholine *N*-Oxide Adducts 7−9

	ν_{NO} (cm^{-1})	
compound	exptl	calcd
NMMO	985, 932	974, 919
7	975,[a] 905	984, 915
8	984, 903	984, 915
9	970,[a] 895	982, 912

[a]Overlap.

giving an absorbance at 907 cm^{-1}; however, in that case the higher energy stretch was also shifted lower to 937 cm^{-1}. Only small changes were observed on comparison of the N−O vibrational modes in **7**−**9**, consistent with the nearly identical calculated vibrational modes.

In order to elucidate the electronic structures of compounds **1**−**9**, these were analyzed by DFT. The optimized structures, frontier molecular orbitals, Te lone pair orbitals, SFO compositions, and energy levels for compounds **1**−**3** are shown in Figure 5, for **4**−**6** in Figure 6, and for **7**−**9** in Figure 7. For compounds **1**−**3**, the molecular orbital energies increase in stability (become more negative) as the ligand changes from donating (^{t}Bu) to withdrawing (Cl_4) in character. The highest occupied molecular orbital (HOMO) for **1** is −5.76 eV, for **2** it is −6.09 eV, and for **3** it is −6.76 eV. A similar trend is observed for their lowest occupied molecular orbitals (LUMOs), with **1** at −3.00 eV, **2** at −3.26 eV, and **3** at −4.10 eV. However, the HOMO−LUMO gap increases on going from 2.76 eV for **1** to 2.84 eV for **2** but then decreases to 2.66 eV for **3**. This trend holds for **7**−**9**, but not for **4**−**6**. The tellurium contribution to the HOMO for compounds **1**−**9** is 0, as the lone pair is energetically buried below the HOMO. For **1**, the HOMO−Te lone pair energy difference is 2.32 eV, which then increases for **2** to 2.49 eV and for **3** to 2.81 eV. With the PyNO ligand, this trend reverses, as the lone pair energy difference is much less for **4** at 1.81 eV, for **5** at 1.70 eV, and for **6** at 1.65 eV; compound **6** possess a second, deeper lone pair contribution 2.55 eV from the HOMO energy. The tellurium lone pair SFO makeup is composed of s, p_x, p_y, and p_z orbitals, each contributing about 1−3% to the total orbital. In contrast, the LUMOs have significantly higher tellurium contributions: for **1**−**3** and **7**−**9** these are ∼80% of the total and 20−30% for **4**−**6**. The availability of tellurium components in the LUMO implies that electrons can be added to the metal center upon reduction, while their absence in the HOMO suggests that holes can be created upon oxidation, but even then the ligand will play the major role. The NMMO ligand increases the Te SFO contributions in the occupied lone pairs, thanks to the methyl substituent on the ligand that acts as a weak electron donor and thereby populates those states.

Bond orders were analyzed using the Mayer, Gopinathan−Jug (G-J) and first Nalewajski−Mrozek (N-M1) indices. The bond orders for compounds **2**, **5**, and **8** are presented in Figure 8, with those of the other complexes in Figures S48−S56 in the Supporting Information. These formalisms consistently give bond orders N-M1 > Mayer > G-J. The catechol bond lengths are ∼2 Å, yet the bond orders are consistently less than 1. The bond lengths for the PyNO and NMMO adducts are longer, whereas the bond orders are much smaller, between 0.1 and 0.3.

Electrostatic potential energy maps were computed to qualitatively relay the bonding nature of the ligands (Figure S57). The energy maps occupy relatively less space around the

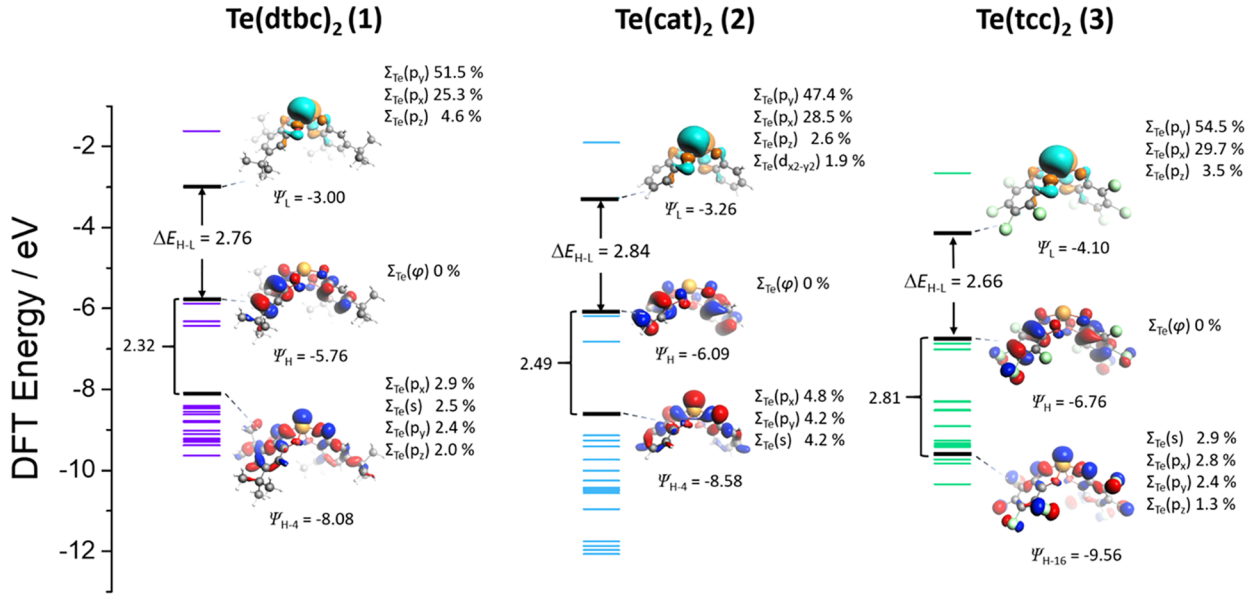

Figure 5. Frontier molecular orbitals, Te lone pair orbitals, and energy levels for **1**−**3**.

https://dx.doi.org/10.1021/acs.inorgchem.1c00126
Inorg. Chem. 2021, 60, 3460−3470

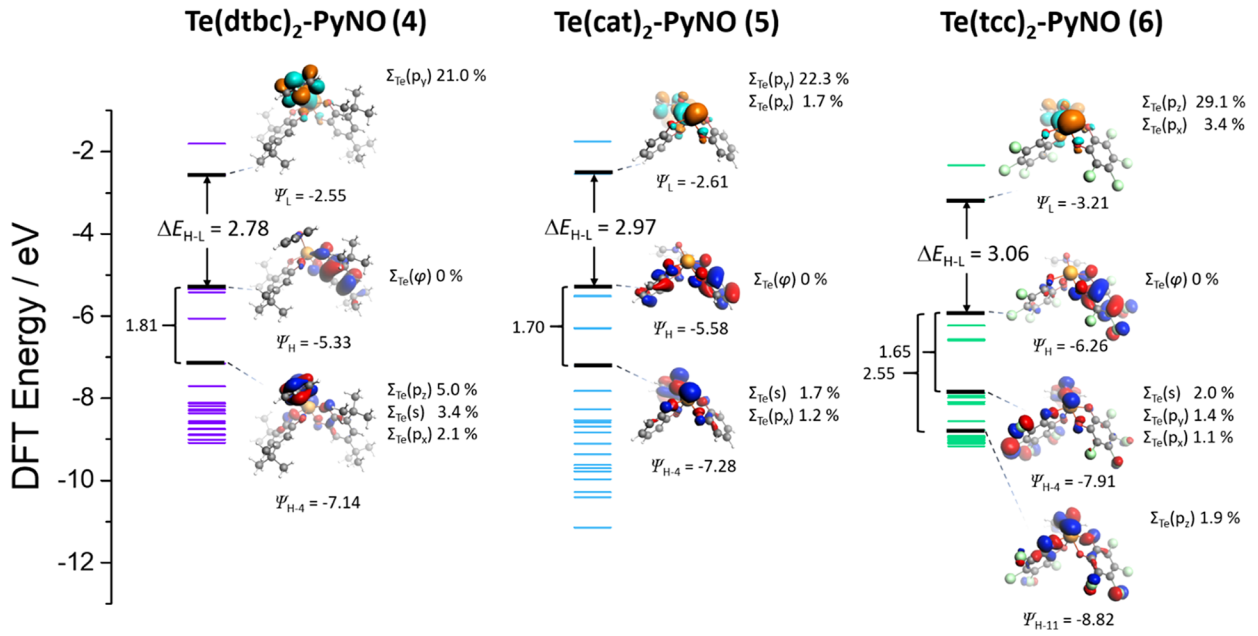

Figure 6. Frontier molecular orbitals, Te lone pair orbitals, and energy levels for **4**–**6**. There is more than one Te lone pair orbital, arising from increased hybridization with the ligand environment.

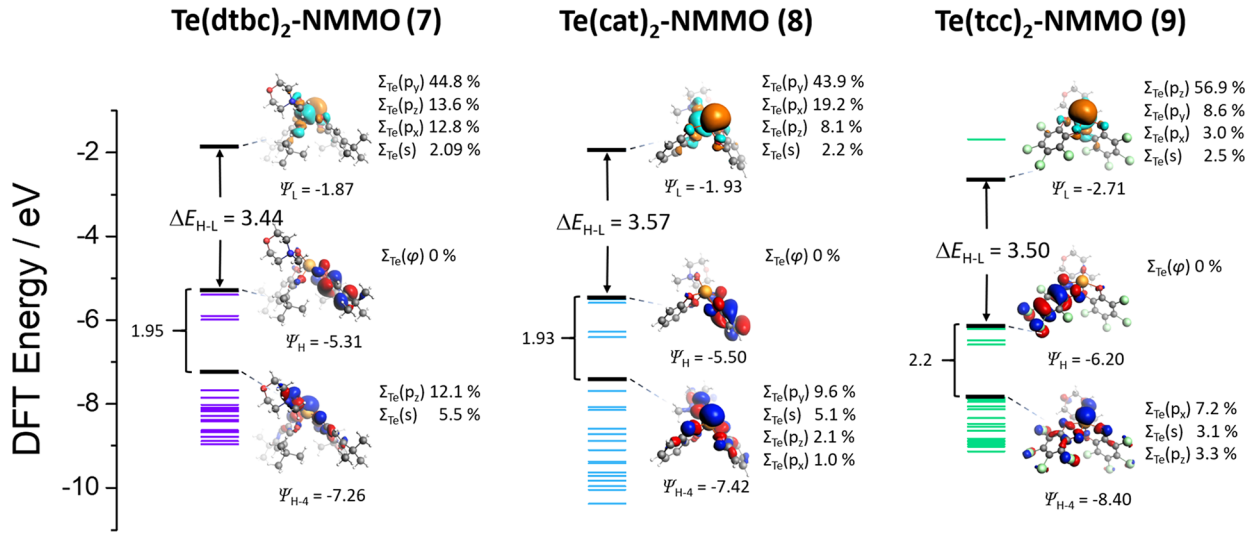

Figure 7. Frontier molecular orbitals, energy levels, Te lone pair orbitals, and Te orbital decomposition for **7**–**9**.

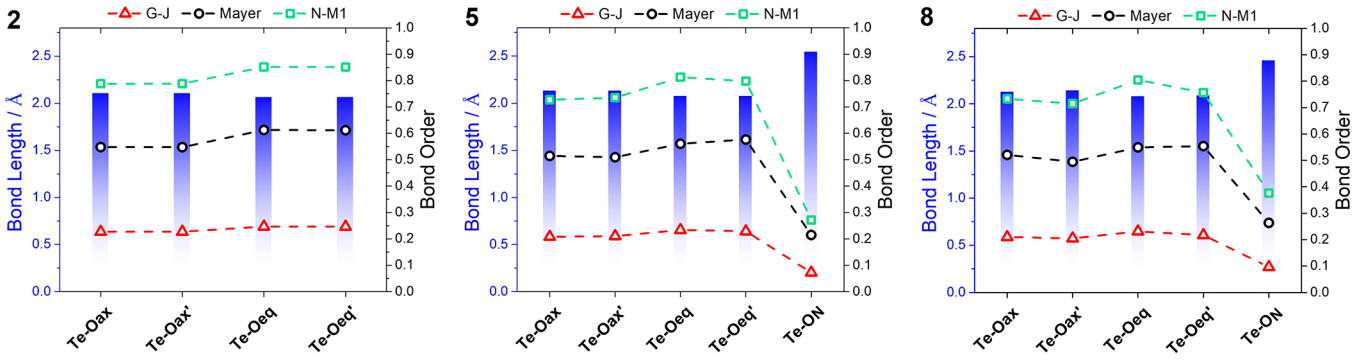

Figure 8. Te–O bond order analyses for selected compounds **2**, **5**, and **8**; all are presented in Figures S48–S56 in the Supporting Information. For each panel, the bar graph is for the left axis (bond lengths in Å) and the dashed lines are for the right axis (bond orders), according to the three selected formalisms of Mayer, Gopinathan–Jug (G-J) and first Nalewajski–Mrozek (N-M1).

https://dx.doi.org/10.1021/acs.inorgchem.1c00126
Inorg. Chem. 2021, 60, 3460–3470

Te−PyNO and Te−NMMO bonds, agreeing with the bond orders that this is a relatively weak interaction.

CONCLUSION

The synthesis and characterization of tellurium complexes featuring three different catecholate ligands have been detailed herein. These have been generated from a variety of tellurium starting materials, including elemental tellurium. Despite the number of oxidation states available to this element, all of the derivatives that were studied were characterized as Te(IV). Addition of strong oxidizers to these complexes resulted in oxidation of the ligand, not the tellurium center. Oxidation products were either a new adduct of the bis(catecholate)-tellurium compound or TeO_2 and the quinone ligand, which resulted from complete oxidation of the catecholate ligand.

The DFT calculations revealed that the tellurium lone pair is energetically buried below the HOMO level, confirming the experimental results that the ligands are noninnocent. The Te−O bond orders are remarkably low, <1, yet the complexes are relatively stable with HOMO−LUMO gaps of 2−3 eV. Overall, the synthetic methods described here are improved and facile routes to these compounds. Moreover, the interesting nature of these complexes mandates them to further analyses with applications toward tellurium extraction from used photovoltaic materials.

ASSOCIATED CONTENT

Supporting Information

The Supporting Information is available free of charge at https://pubs.acs.org/doi/10.1021/acs.inorgchem.1c00126.

Cartesian coordinates, bond analysis, atomic charges, NMR and IR spectra, and X-ray structures and crystallographic data (PDF)

Accession Codes

CCDC 2038732−2038740 contain the supplementary crystallographic data for this paper. These data can be obtained free of charge via www.ccdc.cam.ac.uk/data_request/cif, or by emailing data_request@ccdc.cam.ac.uk, or by contacting The Cambridge Crystallographic Data Centre, 12 Union Road, Cambridge CB2 1EZ, UK; fax: +44 1223 336033.

AUTHOR INFORMATION

Corresponding Author

Suzanne C. Bart − *H. C. Brown Laboratory, Department of Chemistry, Purdue University, West Lafayette, Indiana 47907, United States;* orcid.org/0000-0002-8918-9051; Email: sbart@purdue.edu

Authors

Jerod M. Kieser − *H. C. Brown Laboratory, Department of Chemistry, Purdue University, West Lafayette, Indiana 47907, United States*

Leighton O. Jones − *Department of Chemistry, Northwestern University, Evanston, Illinois 60208, United States;* orcid.org/0000-0001-6657-2632

Nathan J. Lin − *H. C. Brown Laboratory, Department of Chemistry, Purdue University, West Lafayette, Indiana 47907, United States*

Matthias Zeller − *H. C. Brown Laboratory, Department of Chemistry, Purdue University, West Lafayette, Indiana 47907, United States;* orcid.org/0000-0002-3305-852X

George C. Schatz − *Department of Chemistry, Northwestern University, Evanston, Illinois 60208, United States;* orcid.org/0000-0001-5837-4740

Complete contact information is available at: https://pubs.acs.org/10.1021/acs.inorgchem.1c00126

Notes

The authors declare no competing financial interest.

ACKNOWLEDGMENTS

This research work was funded by the Center for Sustainable Separations of Metals (CSSM), a National Science Foundation (NSF) Center for Chemical Innovation (CCI), grant number CHE-1925708. This research was also supported in part by the National Science Foundation through the Major Research Instrumentation Program under Grant No. CHE 1625543 for single crystal X-ray crystallography. Computational resources and staff contributions provided for the Quest High Performance Computing Facility at Northwestern University, which is jointly supported by the Office of the Provost, the Office for Research, and Northwestern University Information Technology.

REFERENCES

(1) Greenwood, N. N.; Earnshaw, A. *Chemistry of the Elements*, 2nd ed.; Elsevier: 1997.

(2) Knockaert, G. Tellurium and Tellurium Compounds. In *Ullmann's Encyclopedia of Industrial Chemistry*; Wiley-VCH: Weinheim, Germany, 2011; Vol. *16*.

(3) Shida, N.; Nishiyama, H.; Zheng, F.; Ye, S.; Seferos, D. S.; Tomita, I.; Inagi, S. Redox Chemistry of π-Extended Tellurophenes. *Commun. Chem.* **2019**, *2*, 124.

(4) Lin, T.-P.; Gabbaï, F. P. Telluronium Ions as σ-Acceptor Ligands. *Angew. Chem., Int. Ed.* **2013**, *52*, 3864−3868.

(5) Zhou, B.; Gabbaï, F. P. Redox-Controlled Chalcogen-Bonding at Tellurium: Impact on Lewis Acidity and Chloride Anion Transport Properties. *Chem. Sci.* **2020**, *11*, 7495−7500.

(6) Antikainen, P. J.; Mälkönen, P. J. Darstellung Und Thermogravimetrische Untersuchung Einer Neuen Tellur—Brenzcatechin-Verbindung. *Z. Anorg. Allg. Chem.* **1959**, *299*, 292−296.

(7) Mbbabazi, J.; Popiel, W. J. Complex Formation between Telluric Acid and Dihydroxybenzenes in Aqueous Solution. *J. Inorg. Nucl. Chem.* **1979**, *41*, 1491−1493.

(8) Annan, T. A.; Ozarowski, A.; Tian, Z.; Tuck, D. G. The Reaction of Some Substituted Ortho-Benzoquinones with Elemental Tellurium and with Tellurium(II) Compounds. *J. Chem. Soc., Dalton Trans.* **1992**, 2931.

(9) Drabowicz, J.; Lewkowski, J.; Kudelska, W.; Girek, T. Product Class 28: Acyclic Dialkyl Tellurones and Derivatives. In *Science of Synthesis*; Thieme: 2008; Vol. *39*, pp 1111−1116.

(10) Shimizu, T.; Kamigata, N. Product Class 30: Acyclic Dialkyl Telluroxides and Derivatives. In *Science of Synthesis*; Thieme: 2008; Vol. *39*, pp 1127−1135.

(11) Carrera, E. I.; Seferos, D. S. Efficient Halogen Photoelimination from Dibromo, Dichloro and Difluoro Tellurophenes. *Dalton Trans.* **2015**, *44*, 2092−2096.

(12) Carrera, E. I.; McCormick, T. M.; Kapp, M. J.; Lough, A. J.; Seferos, D. S. Thermal and Photoreductive Elimination from the Tellurium Center of π-Conjugated Tellurophenes. *Inorg. Chem.* **2013**, *52*, 13779−13790.

(13) Jahnke, A. A.; Howe, G. W.; Seferos, D. S. Polytellurophenes with Properties Controlled by Tellurium-Coordination. *Angew. Chem., Int. Ed.* **2010**, *49*, 10140−10144.

(14) Fujihara, H.; Takaguchi, Y.; Ninoi, T.; Erata, T.; Furukawa, N. Preparation and Characterization of a Four-Coordinated Ditellurane Stabilized by a Transannular Tellurium−Tellurium Bond from 1,5-

Ditelluracyclooctane: A New Multicentre Hypervalent Species. *J. Chem. Soc., Perkin Trans. 1* **1992**, 2583−2584.
(15) Fujihara, H.; Ninoi, T.; Akaishi, R.; Erata, T.; Furukawa, N. First Example of Tetraalkyl Substituted Ditelluride Dication Salt from 1,5-Ditelluracyclooctane. *Tetrahedron Lett.* **1991**, *32*, 4537−4540.
(16) Yang, H.; Lin, T.-P.; Gabbaï, F. P. Telluroether to Telluroxide Conversion in the Coordination Sphere of a Metal: Oxidation-Induced Umpolung of a Te−Au Bond. *Organometallics* **2014**, *33*, 4368−4373.
(17) Lin, T.-P.; Gabbaï, F. P. Two-Electron Redox Chemistry at the Dinuclear Core of a TePt Platform: Chlorine Photoreductive Elimination and Isolation of a Te V Pt I Complex. *J. Am. Chem. Soc.* **2012**, *134*, 12230−12238.
(18) Pangborn, A. B.; Giardello, M. A.; Grubbs, R. H.; Rosen, R. K.; Timmers, F. J. Safe and Convenient Procedure for Solvent Purification. *Organometallics* **1996**, *15*, 1518−1520.
(19) Rodger, C.; Sheppard, N.; McFarlane, C.; McFarlane, W. Group VI-Oxygen, Sulphur, Selenium and Tellurium. In *NMR and the Periodic Table*; Harris, R. K., Mann, B. E., Eds.; Academic Press: London, 1978; pp 383−419.
(20) te Velde, G.; Bickelhaupt, F. M.; Baerends, E. J.; Fonseca Guerra, C.; van Gisbergen, S. J. A.; Snijders, J. G.; Ziegler, T. Chemistry with ADF. *J. Comput. Chem.* **2001**, *22*, 931−967.
(21) Becke, A. D. Density-functional Thermochemistry. III. The Role of Exact Exchange. *J. Chem. Phys.* **1993**, *98*, 5648−5652.
(22) Stephens, P. J.; Devlin, F. J.; Chabalowski, C. F.; Frisch, M. J. Ab Initio Calculation of Vibrational Absorption and Circular Dichroism Spectra Using Density Functional Force Fields. *J. Phys. Chem.* **1994**, *98*, 11623−11627.
(23) Van Lenthe, E.; Baerends, E. J. Optimized Slater-Type Basis Sets for the Elements 1−118. *J. Comput. Chem.* **2003**, *24*, 1142−1156.
(24) Franchini, M.; Philipsen, P. H. T.; Visscher, L. The Becke Fuzzy Cells Integration Scheme in the Amsterdam Density Functional Program Suite. *J. Comput. Chem.* **2013**, *34*, 1819−1827.
(25) van Lenthe, E.; Ehlers, A.; Baerends, E.-J. Geometry Optimizations in the Zero Order Regular Approximation for Relativistic Effects. *J. Chem. Phys.* **1999**, *110*, 8943−8953.
(26) Mayer, I. Charge, Bond Order and Valence in the AB Initio SCF Theory. *Chem. Phys. Lett.* **1983**, *97*, 270−274.
(27) Gopinathan, M. S.; Jug, K. Valency. I. A Quantum Chemical Definition and Properties. *Theor. Chim. Acta* **1983**, *63*, 497−509.
(28) Nalewajski, R. F.; Mrozek, J. Modified Valence Indices from the Two-Particle Density Matrix. *Int. J. Quantum Chem.* **1994**, *51*, 187−200.
(29) Nalewajski, R. F.; Mrozek, J.; Michalak, A. Two-Electron Valence Indices from the Kohn-Sham Orbitals. *Int. J. Quantum Chem.* **1997**, *61*, 589−601.
(30) Badesha, S. S.; Monczka, P.; Smith, S. D. Chalcogenide Esters as Reactive Intermediates in Selenium and Tellurium Purifications. *Can. J. Chem.* **1983**, *61*, 2199−2202.
(31) Taylor, P.; Defilippo, M. Process to Recycle End of Life CdTe Modules and Manufacturing Scrap. US20120325676A1, 2012.
(32) Aebisher, D.; Brzostowska, E. M.; Mahendran, A.; Greer, A. Regioselective (Biomimetic) Synthesis of a Pentasulfane from Ortho -Benzoquinone. *J. Org. Chem.* **2007**, *72*, 2951−2955.
(33) Perkins, C. W.; Martin, J. C.; Arduengo, A. J.; Lau, W.; Alegria, A.; Kochi, J. K. An Electrically Neutral σ-Sulfuranyl Radical from the Homolysis of a Perester with Neighboring Sulfenyl Sulfur: 9-S-3 Species. *J. Am. Chem. Soc.* **1980**, *102*, 7753−7759.
(34) Lindqvist, O.; et al. The Crystal Structure of Tellurium(IV) Catecholate, Te(C6H4O2)2. *Acta Chem. Scand.* **1967**, *21*, 1473−1483.
(35) Holmes, R. R.; Day, R. O.; Sau, A. C.; Poutasse, C. A.; Holmes, J. M. Stereochemicaly Nonrigid Five-Coordinated Germanates. Synthesis and Structure of Hydroxy-and Halo-Containing Spirocyclic Germanium(IV) Complexes. *Inorg. Chem.* **1985**, *24*, 193−199.
(36) Holmes, R. R.; Day, R. O.; Sau, A. C.; Holmes, J. M. Distortion Coordinate for Nonrigid Five-Coordinated Germanium. Synthesis and Molecular Structure of Spirocyclic Anionic Methylgermanates Varying in Ring Composition. *Inorg. Chem.* **1986**, *25*, 600−606.
(37) Weiner, H.; Finke, R. G. An All-Inorganic, Polyoxometalate-Based Catechol Dioxygenase That Exhibits > 100 000 Catalytic Turnovers. *J. Am. Chem. Soc.* **1999**, *121*, 9831−9842.
(38) Macdonald, A. L.; Trotter, J. Crystal and Molecular Structure of O-Benzoquinone. *J. Chem. Soc., Perkin Trans. 2* **1973**, 476.
(39) Zanotti, G.; Del Pra, A. The Crystal and Molecular Structure of Tetrachloro- o -Benzoquinone. *Acta Crystallogr., Sect. B: Struct. Crystallogr. Cryst. Chem.* **1978**, *34*, 2997−3001.
(40) Klobukowski, E. R.; Angelici, R. J.; Woo, L. K. Bulk Gold-Catalyzed Oxidations of Amines and Benzyl Alcohol Using Amine N-Oxides as Oxidants. *Catal. Lett.* **2012**, *142*, 161−167.
(41) Marsh, R. E.; Kapon, M.; Hu, S.; Herbstein, F. H. Some 60 New Space-Group Corrections. *Acta Crystallogr., Sect. B: Struct. Sci.* **2002**, *58*, 62−77.
(42) Maia, E.; Peguy, A.; Pérez, S. Cellulose Organic Solvents. I. The Structures of Anhydrous N-Methylmorpholine N-Oxide and N-Methylmorpholine N-Oxide Monohydrate. *Acta Crystallogr., Sect. B: Struct. Crystallogr. Cryst. Chem.* **1981**, *37*, 1858−1862.
(43) Murthy, P. R.; Patel, C. C. Pyridine N-Oxide Complexes of Zirconyl, Thorium, and Uranyl Perchlorates. *Can. J. Chem.* **1964**, *42*, 856−860.
(44) Kakiuti, Y.; Kida, S.; Quagliano, J. V. Metal-Ligand Stretching, N-O Stretching and C-H Out-of-Plane Bending Vibrations of Pyridine N-Oxide and Hexakis (Pyridine N-Oxide) Metal Perchlorates. *Spectrochim. Acta* **1963**, *19*, 201−211.
(45) Fernandes, L. C.; Matos, J. R.; Zinner, L. B.; Vicentini, G.; Zukerman-Schpector, J. Crystal Structures, Spectroscopic, TG and DSC Studies of Lanthanide Picrate Complexes with 4-Methylmorpholine N-Oxide (MMNO). *Polyhedron* **2000**, *19*, 2313−2318.
(46) Maï, P. T.; Herzog-Cance, M.-H.; Potier, A.; Potier, J. Étude, Par Spectroscopie de Vibration, de Deux Solvants de La Cellulose: La N -Méthyl Morpholine N -Oxyde et Son Monohydrate. *Can. J. Chem.* **1982**, *60*, 2777−2784.

https://dx.doi.org/10.1021/acs.inorgchem.1c00126
Inorg. Chem. 2021, 60, 3460−3470